Journal of Engineering and Technology for Industrial Applications

ISSN ONLINE: 2447-0228

ITEGAM-JETIA

Manaus, v.12 n.58, p. 621-634. March/April, 2026.

DOI: https://doi.org/10.5935/jetia.v12i58.3207

RESEARCH ARTICLE OPEN ACCESS

# RED-TAILED HAWK (RTH) ALGORITHM FOR OPTIMAL PV RECONFIGURATION IN IRRIGATION SYSTEMS UNDER PARTIAL SHADING CONDITIONS

**Abdelouaoud Loukriz*[1], Abderrahim Zemmit[2], Ahmed Bendib[3], Moadh Kichen[4]**

[1]Electrical Engineering Department, University of Science and Technology Houari Boumediene, Algiers, 16111, Algeria.
[2, 3]Electrical Engineering Department, University of M'sila, 28000, Algeria.
[4]Electrical Engineering Department, University of Science and Technology of Oran, Oran, 16111, Algeria.

[1]https://orcid.org/0000-0001-6558-5933, [2]http://orcid.org/0000-0002-2365-0378
[3]https://orcid.org/0000-0002-7689-8692, [4]http://orcid.org/0009-0001-8072-1689

Email: *abdelouadoud.loukriz@usthb.edu.dz

**ARTICLE INFO**

***Article History***
Received: December 11, 2025
Reviewed: January 1, 2026
Accepted: January 19, 2026
Published: March 31, 2026

***Keywords:***
Photovoltaic,
Agricultural water pumping systems (AWPS),
Partial shading conditions (PSCs),
Brushless DC (BLDC) motor,
Red-tailed hawk (RTH),

**ABSTRACT**

Photovoltaic (PV) water pumping systems offer a sustainable solution for agricultural irrigation in regions where conventional energy sources are unreliable or expensive. However, partial shading (PS) significantly degrades PV performance and limits water delivery. This paper proposes a dynamic PV array reconfiguration strategy based on the Red-Tailed Hawk (RTH) optimization algorithm to mitigate PS effects. The reconfigured PV array, combined with maximum power point tracking (MPPT), supplies a brushless DC (BLDC) motor-driven water pumping system to enhance operational efficiency. The proposed method ensures stable steady-state operation while maintaining the PV system near the maximum power point under varying shading conditions. Performance evaluation is carried out in MATLAB using a 4×5 PV array subjected to dynamic shading caused by a tree, with comparisons made against the conventional total cross-tied (TCT) configuration using reported experimental data. The results demonstrate clear improvements in water flow, with average gains of 36 liters per hour in the first case and 111.6 liters per hour in the second case. These outcomes confirm the effectiveness of the proposed approach and highlight its potential for improving the sustainability and reliability of photovoltaic water pumping systems in energy-constrained agricultural regions.



## I. INTRODUCTION

Innovation and technology are essential in enhancing agricultural productivity. A noteworthy domain where substantial advancements are occurring is the incorporation of renewable energy sources (RESs) into agriculture, a highly significant trend. Agriculture is a vital industry in numerous countries, playing a crucial role in their economies. Currently, a significant proportion of farmers depend on conventional sources such as mains power or diesel engines to fulfill their water pumping requirements [1]. Nevertheless, the cost of fuel pumping has become progressively burdensome. Furthermore, expansive stretches of agricultural land are situated in isolated regions devoid of electrical infrastructure [2], [3]. Even in regions with electrical availability, the demand for water rises throughout the summer season, frequently aligning with power outages. Therefore, the use of PV water pumping emerges as a viable remedy to conserve energy, alleviate strain on the power grid, and diminish long-term energy expenses. However, partial shading is a significant obstacle to the effectiveness of solar water pumping systems, and addressing this issue is a challenge. The PS is commonly attributed to obstructions such as trees, dense vegetation, shrubs, utility poles, avian presence, topographical elevations, and rocks that create shadows on adjacent PV modules [4], [5]. Consistent shading of PV modules in a certain location can result in the formation of localized areas of high temperature, known as hot spots, which can potentially cause harm or damage. In order to alleviate this issue, bypass diodes are typically fitted on PV modules to prevent this occurrence.

Nevertheless, this arrangement frequently results in many peaks in the PV output, which substantially diminishes the total generated power of the PV array [6]. In this regard, several PV array configurations, including TCT (total-cross-tied) and HC (honeycomb), have been created to reduce mismatch losses and enhance efficiency. TCT topology has demonstrated the maximum power production in the majority of shading scenarios [6], [7]. However, no one topology consistently surpasses the others in every partial shading condition (PSC). To this end, numerous techniques for modifying the arrangement of PV arrays have been suggested in academic literature to enhance their power generation [8]. Static reconfiguration methods use fixed patterns to reduce shading effects and work well for predictable shading [9]. With modern sensors and processors, dynamic reconfiguration has emerged as an effective solution for variable shading conditions[9], [10]. Applied to TCT PV arrays, it balances irradiance to enhance power output [11], [12] , improving PV water pumping system efficiency. Dynamic reconfiguration is particularly suited for smaller PV arrays, stabilizing P–V characteristics and enabling conventional MPPT techniques to maximize energy extraction [13]. Many PV reconfiguration methods leverage various optimization algorithms, each exhibiting distinct strengths and weaknesses. Fathy's [14] butterfly optimization algorithm efficiently enhances power generation by structural redesign, yet it may struggle with computational complexity for large-scale arrays.

The democratic political approach [15] improves efficiency but may face scalability issues in larger systems. The grasshopper optimizer [16] shows promise in partial shading scenarios but can suffer from slow convergence rates. ACO [17] maximizes power extraction well but requires significant computational resources for larger arrays. The ken-ken puzzle method [18] is innovative in reconnecting shaded panels but might not always find the global optimum. Genetic Algorithms (GA) [19] are robust and versatile, though they can be computationally intensive and may converge to local optima. The Vommi optimization algorithm [20] maximizes power extraction efficiently but may require fine-tuning for different conditions. Particle Swarm Optimization (PSO)[21] is effective but can struggle with early convergence to suboptimal solutions. The Harris Hawks Optimizer (HHO)[22] provides good performance but lacks robustness in complex optimization challenges. Finally, the Honey Badger Algorithm (HBA)[23] and Artificial Bee Colony (ABC) [24] offer advanced methods but face issues such as prolonged convergence times, vulnerability to local optima, and high computational demands. Numerous researchers have explored PVWPSs, highlighting two main configurations: single-stage and two-stage configurations [25], [26]. In a single-stage configuration, regulating the DC link is complex [26].

Despite this complexity, single-stage topologies are considered more efficient due to their reduced number of components [27]. However, the two-stage power conversion approach offers greater flexibility in design, operation, and control. PVWPSs utilizing AC motors, particularly induction motors (IM), are often preferred due to their reliability, lower costs, and minimal maintenance requirements. Conversely, DC motors are typically employed in low-power solar PV water pumps [28]. Despite their usage, DC motors with brushes suffer from low efficiency and demand frequent maintenance because of the sliding brush contacts and the commutator. In contrast, three-phase brushless direct-current (BLDC) motors emerge as suitable alternatives owing to their high efficiency, compact design, and ease of operation [29]. Over the past decade, these attributes have made BLDC motors increasingly popular for water pumping applications, highlighting their advantageous characteristics in this specific field [28]. Although the wide PV reconfiguration techniques, their application for PVWPSs have not been addressed yet. To this end, a new dynamic PV array reconfiguration based on the RTH algorithm intended for a PVWPS considering PS is proposed in this paper. The main objective of this work is to improve the water flow of a PVWPS operating under PSCs. The main papers' contributions are:

- An innovative dynamic PV reconfiguration based on the RTH optimization algorithm is proposed. The RTH uses real-time irradiation data to reconfigure the modules within a PV array using switches, considering PSCs.
- The reconfigured PV array controlled by a P&O MPPT technique is applied for a water pumping system driven by a BLDC motor. The proposed algorithm allows the conventional P&O MPPT algorithms to perform optimally in achieving the global maximum power point even under PSCs, hence improving power and system performance.
- A comprehensive comparative study demonstrates the effectiveness of the proposed approach, showing clear improvements in water flow with average gains of 36 liters per hour in the first operating case and 111.6 liters per hour in the second case, compared to the conventional total cross-tied (TCT) configuration.

The paper's remainder is structured as follows: Section II presents the configuration and modeling of the system under study. Section III describes the proposed PV reconfiguration approach. The simulation results are discussed in Section IV. Finally, Section V ends with a conclusion.

## II. PVWPS CONFIGURATION AND MODELING

The schematic diagram of the PVWPS under study is illustrated in Figure 1, highlighting essential elements such as a partially shaded TCT PV array, a switching matrix, power electronic converters (including a DC-DC boost converter and a DC-AC two-level inverter), a BLDC motor, and a pump with its associated control system. Additionally, it highlights the proposed RTH optimization algorithm, introduced to mitigate the PS effect by controlling the switching matrix. Furthermore, the MPPT controller used to track the PV MPP by controlling the DC-DC converter via PWM is also presented in this scheme. The modeling of elements included in the PVWPS is provided in the following paragraphs.

### II.1 BLDC MOTOR

The mathematical model of the BLDC motor can be derived using the same approach as that of a three-phase synchronous machine. Thus, the equivalent circuit of the armature winding model for the BLDC motor can be defined as follows [30]:

$$\begin{cases} v_a = R.i_a + L\frac{di_a}{dt} + e_a \\ v_b = R.i_b + L\frac{di_b}{dt} + e_b \\ v_c = R.i_c + L\frac{di_c}{dt} + e_c \end{cases} \quad (1)$$

Where $v_{abc}$ and $i_{abc}$ denote the three-phase voltages and currents, $R$ and $L$ are the stator resistance and inductance, and $e_{abc}$ are the motor voltages. Inputs to the BLDC motor control block include the Hall sequence number or rotor position from sensors like Hall effect sensors or encoders, along with torque direction. This information determines the rotor's sector position, enabling the calculation of the appropriate switching sequence. This sequence energizes motor phases to maintain a torque angle of 90 degrees (with a 30-degree deviation) relative to the stator magnetic field. For instance, Hall states that 5 triggers phase *A* and *C* to initiate motor rotation, optimizing efficiency as shown in Figure 2. While the calibration of the Hall sensor sequence ensures precise commutation logic, as detailed in Table 1.

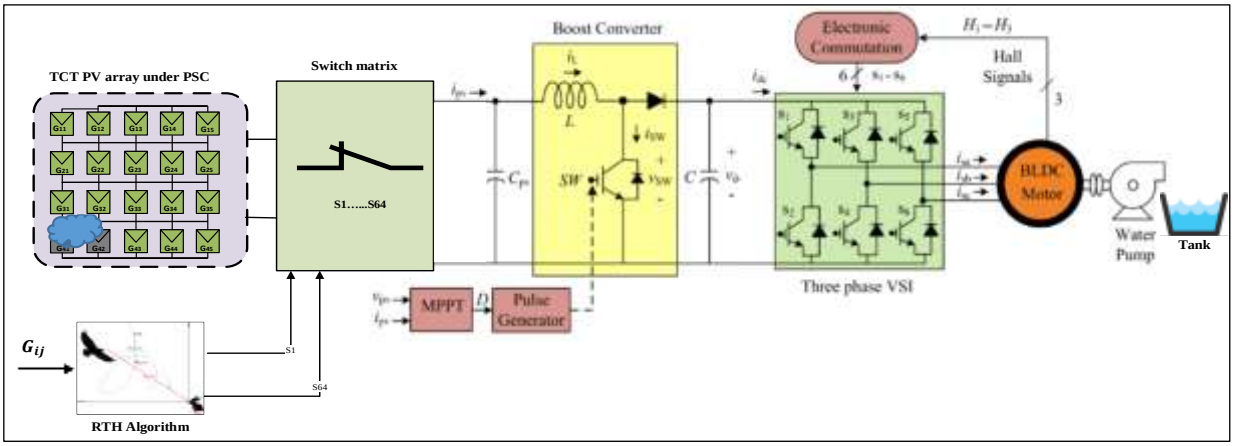


Figure 1: Schematic diagram of the PVWPS with the proposed reconfiguration-based RTH algorithm.
Source: Authors, (2026).

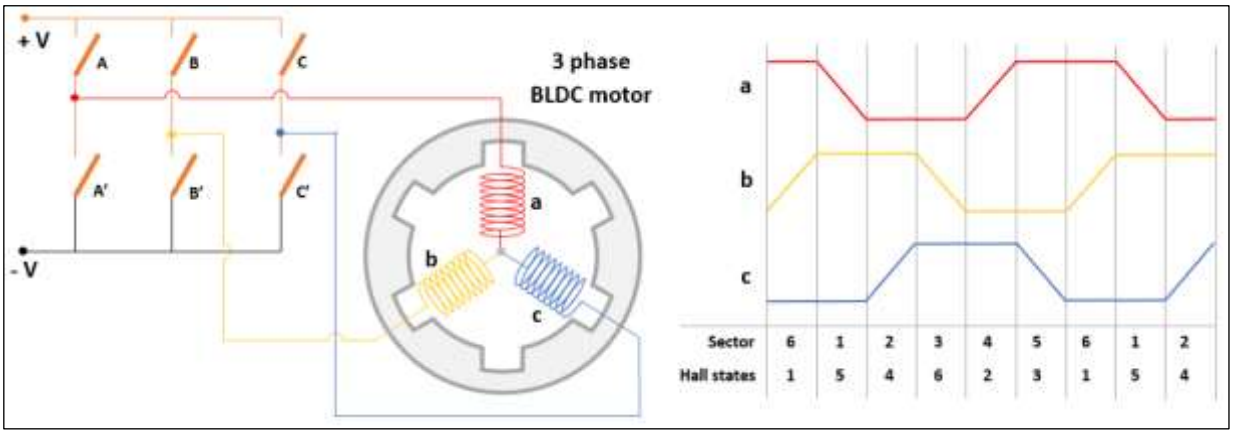


Figure 2: Simplified circuit diagram illustrating the control of BLDC motor phases via a three-phase bridge.
Source: Authors, (2026).

Table 1: Calibration of the Hall sensor sequence ensures precise commutation logic.

| Position ($\theta$) | Sector | Switching Sequence (AA' BB' CC') | | |
|---|---|---|---|---|
| | | **AA'** | **BB'** | **CC'** |
| **[-30°, 30°]** | 1 | 00 | 10 | 01 |
| **[30°, 90°]** | 2 | 01 | 10 | 00 |
| **[90°, 150°]** | 3 | 01 | 00 | 10 |
| **[150°, 210°]** | 4 | 00 | 01 | 10 |
| **[210°, 270°]** | 5 | 10 | 01 | 00 |
| **[270°, 330°]** | 6 | 10 | 00 | 01 |

Source: Authors, (2026).

## II.2 PV ARRAY MODELING

To guarantee that the PVWPS operates correctly, it is imperative that the power capacity of the PV array should be greater than that of the induction motor. In this regard, a TCT (4×4) PV array of 2.4 kW capacity is chosen to supply the BLDC induction motor. The TCT array current is calculated using the method described as [31]:

$$I_{ij(shaded)} = K.I_{ij(STC)} \quad (2)$$

with:

$$K = \frac{G_{ij}}{G_{STC}} \quad (3)$$

Being $i$ and $j$ the row and column number of an array, $I_{ij(shaded)}$ and $I_{ij(standard)}$ represent the module current, during shaded and standard irradiance (i.e., 1000 $W/m^2$), $G_{ij}$ is the irradiance received by the $ij$ module, and $G_{STC}$ denotes the standard irradiance. Besides, the PV array voltage can be derived as follows [5]:

$$V_{PV} = \sum_{i=1}^{m} V_i \quad (4)$$

Where $m$ indicates the total number of rows, $i$ indicates the row number, $V_i$ is the voltage of the $i^{th}$ row, and $V_{pv}$ represents the array voltage. Table 2 lists the specifications of the adopted PV module and the PV array.

Table 2: PV system characteristics.

| Parameter | PV module | PV array |
|---|---|---|
| Maximum power ($P_{mpp}$)[ W] | 150 | 2400 |
| Maximum current ($I_{mpp}$)[A] | 4.35 | 17.4 |
| Maximum voltage ($V_{mpp}$) [V] | 34.6 | 138.4 |
| Open circuit voltage ($V_{ov}$) [V] | 43.6 | 174.4 |
| Short circuit current ($I_{sc}$) [A] | 4.85 | 19.4 |

Source: Authors, (2026).

## II.3 DC-DC BOOST CONVERTER

The design of the converter plays a vital role in deciding the performance of the system. The values of $\alpha$, $L_{pv}$, and $C_{dc}$ parameters of the boost converter should be calculated using the continuous conduction mode (CCM) [32]. The boost converter duty cycle $\alpha$ can be obtained using the following method:

$$\alpha = \frac{V_{dc} - V_{mppv}}{V_{dc}} \quad (5)$$

The boost converter's inductance can be computed using the equation below:

$$L = \frac{\alpha.V_{mppv}}{f_s.\Delta I} \quad (6)$$

Where $f_s$ is the switching frequency and $\Delta I$ is the current ripple. On the other hand, the DC bus voltage at the inverter input, $V_{dc}$, can be calculated using the following relationship:

$$V_{dc} = \frac{2\sqrt{3}V_{LL}}{\sqrt{3}} \quad (7)$$

With $V_{LL}$ is the RMS line voltage of the induction motor. The capacitor of the DC bus is calculated by:

$$C_{dc} = \frac{6\,\alpha V_{LL} I_L t}{\sqrt{3}\,({V_{dc}}^{*2} - {V_{dc}}^{2})} \quad (8)$$

Where ${V_{dc}}^*$ and $V_{dc}$ are the reference and actual values of the DC bus voltage, respectively, $t$ stands for the time for which the DC link voltage is to be changed, and $I_L$ is the line current.

## II.4 CENTRIFUGAL PUMP MODELLING

The load torque of a centrifugal pump ($T_p$) is proportional to the square of the induction motor speed ($\Omega$), as shown in the equation below [33]:

$$T_p = K_p \Omega^2 \quad (9)$$

where $K_p$ is the proportionality constant that can be determined by the following equation:

$$K_p = P_{np}/\Omega_{rn}^3 \quad (10)$$

The water flow and pressure of the pump are determined by the head of the pump and the mechanical power available at the rotating impeller. The use of affinity laws, which simply necessitate the pump's ratings and actual input parameters such as rotor speed and torque[34], could streamline the calculation of the pump's output characteristics.

$$\begin{cases} H' = (\frac{\Omega_r}{\Omega_{rn}})^2 . H \\ Q' = (\frac{\Omega_r}{\Omega_{rn}})^2 . Q \\ P' = (\frac{\Omega_r}{\Omega_{rn}})^2 . P \end{cases} \quad (11)$$

Where $H$, $Q$, and $P$ represent the rated parameters of the pump when it is operating at the rated speed, $\Omega_{rn}$, while $H'$, $Q'$, and $P'$ represent the parameters of the pump when it is operating at a specified speed, $\Omega_r$.

## III. PROPOSED RTH-BASED PV ARRAY RECONFIGURATION

This section focuses mainly on describing the proposed reconfiguration method based on the RTH optimization algorithm intended for improving the PV-based pumping system working under PSCs. However, before that, the effect of the PS on a PV array is first investigated. In addition, the PO-MPPT controller is highlighted at the end of this section.

### III.1 PARTIAL SHADING EFFECT

Partial shading in photovoltaic systems causes power losses due to current and voltage mismatches, leading to multiple local maxima on the P–V curve that conventional MPPT algorithms struggle to handle. Shaded modules generate less current, may act as loads, and can develop hot spots that damage the panels. Irradiance variations significantly affect the P–V characteristics, as illustrated in Figure 3.

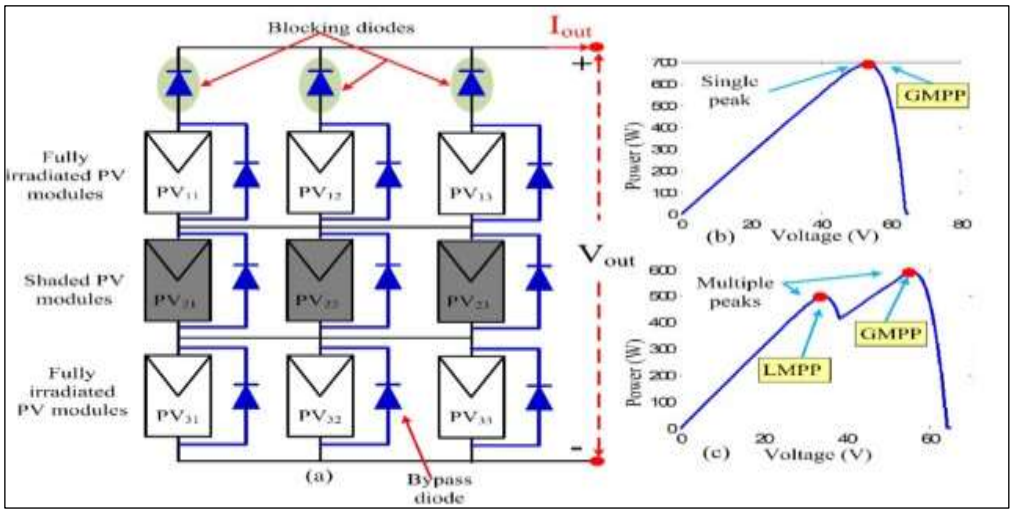


Figure 3: Impact of irradiation changes on the P-V curves: (a) shaded PV structure, (b) uniform irradiation, and (c) PSCs.
Source: Authors, (2026).

### III.2 RTH-BASED PV ARRAY DYNAMIC RECONFIGURATION

This study focuses on a total cross-tied (TCT) PV array configuration due to its ability to maximize power under shading conditions [35]. A dynamic reconfiguration strategy is applied, using irradiance sensor data from each module to control switching. The proposed Red-Tailed Hawk (RTH) algorithm optimally determines PV module configurations to track the maximum power point (MPP). Inspired by the hunting behavior of red-tailed hawks, the RTH algorithm combines evolutionary and swarm optimization principles through three main stages—high soaring, low soaring, and stooping—allowing efficient and adaptive problem-solving for complex PV reconfiguration tasks:

i) It starts with a high-soaring phase, akin to how evolutionary algorithms search for solutions in a broad space initially [2]. Figure 4(a) illustrates the behavior of the red-tailed hawks during the high soaring stage, and (11) represents the mathematical model of this stage:

$$X(t) = Xbest + \big(Xmean - X(t-1)\big). Levy(\dim). \mathrm{TF(t)} \quad (12)$$

Where $X(t)$ represents the RTH position at the iteration $t$, $X_{best}$ is the best-obtained position, $X_{mean}$ is the positions' mean, Levy represents the levy flight distribution function that can be calculated according to (15), and $TF(t)$ denotes the transition factor function that can be calculated according to (14).

$$Levy(\dim) = s\frac{\mu.\sigma}{|v|^{\beta-1}} \quad (13)$$

with

$$\sigma = \left( \frac{\Gamma(1+\beta).\sin(\frac{\pi\beta}{2})}{\Gamma(1+\beta/2).\beta.2^{(1-\beta/2)}} \right)$$

$$\mathrm{TF(t)} = 1 + \sin\left(2.5 + \left(\frac{\mathrm{t}}{T_{max}}\right)\right) \tag{14}$$

While *s* is a constant (0.01), *dim* is the problem dimension, $\beta$ is a constant (1.5), *u* and υ are random numbers between 0 and 1, and $T_{max}$ represents the maximum number of iterations.

ii) The second stage involves a gradual descent toward the best solution, emulating the behavior of hawks as they close in on their target during hunting. This phase resembles the systematic exploration of the solution space. This stage is illustrated in Figure 4(b), and its model can be expressed as follows:

$$\mathrm{X(t)} = X_{best} + \big(x(t) + y(t)\big).StepSize(t) \tag{15}$$
$$StepSize(t) = X(t) - X_{mean}$$

where *x* and *y* denote direction coordinates which can be calculated as follows:

$$\begin{cases} x(t) = R(t).\sin(\theta(t)) \\ y(t) = R(t).cos(\theta(t)) \end{cases}; \begin{cases} R(t) = R_0.\left(r - \dfrac{t}{T_{\max}}\right).rand \\ \theta(t) = A.\left(1 - \dfrac{t}{T_{max}}\right).rand \end{cases}; \begin{cases} x(t) = x(t)/max|x(t)| \\ y(t) = y(t)/max|y(t)| \end{cases} \tag{16}$$

Where $R_0$ represents the initial value of the radius [0.5–3], *A* denotes the angle gain [5–15], *rand* is a random gain [0–1], and *r* is a control gain [1, 2]. These parameters help the hawk fly around the prey with spiral movements, as explained in Figure 5(a).

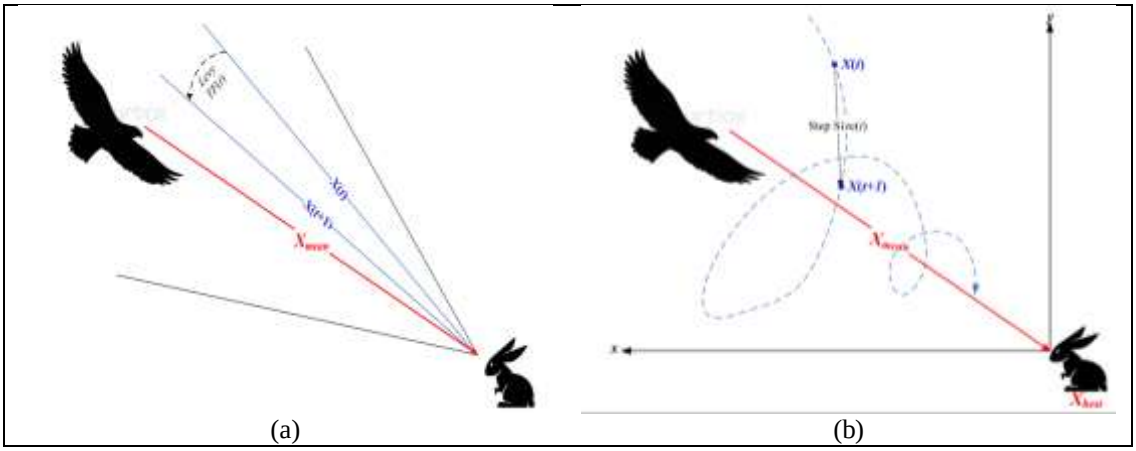

(a) (b)

Figure 4: The behavior of red-tailed hawk during the (a) high soaring stage and (b) low soaring stage.
Source: Authors, (2026).

iii) In the final stage of the algorithm, known as stooping and swooping, the algorithm refines the search around the best solution found so far by incorporating information from previous iterations. This phase represents the focused exploitation of the best regions identified in the search space. This stage can be modeled as follows:

$$X(t) = \alpha(t).X_{best} + x(t).StepSize1(t) + y(t).StepSize2(t) \tag{17}$$

where each step size can be calculated as follows:

$$\begin{cases} StepSize1(t) = X(t) - TF(t).X_{mean} \\ StepSize2(t) = G(t).X(t) - TF(t).X_{best} \end{cases} \tag{18}$$

With $\alpha$ is the hawk's acceleration that increases with the increase of *t* to enhance the convergence speed, and *G* is the gravity effect that decreases to reduce the exploitation diversity when the hawk is much near the prey as Figure 5(b) explains. These parameters are defined as follows:

$$\begin{cases} \alpha(t) = sin^2(2.5 - \frac{t}{T_{max}}) \\ G(t) = 2.(1 - \frac{t}{T_{max}}) \end{cases} \tag{19}$$

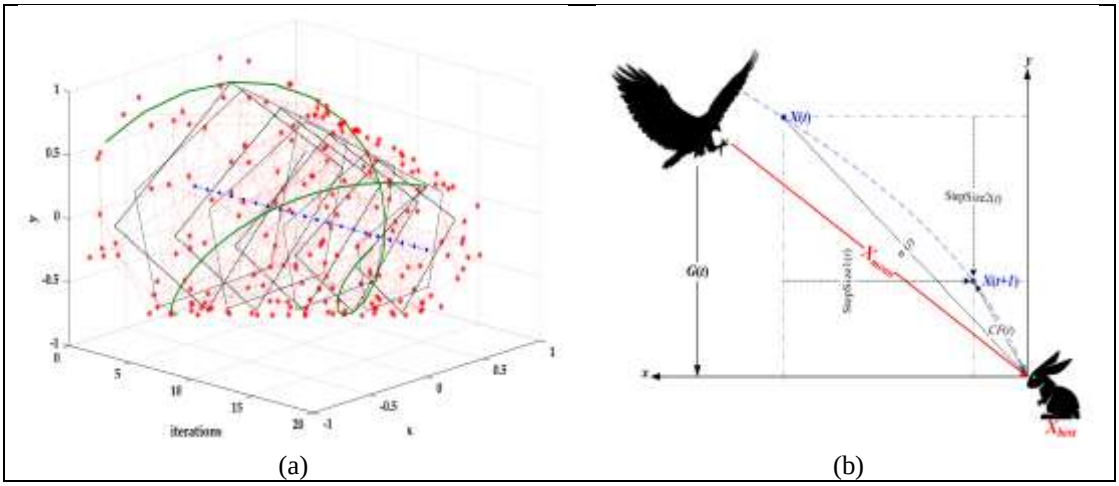


(a) (b)

Figure 5: (a) Evolution of the direction coordinates as a function of iterations and (b) behavior of red-tailed hawk during stooping and swooping stages.
Source: Authors, (2026).

### III.3 APPLICATION OF THE RTH ALGORITHM FOR PV RECONFIGURATION

To apply the proposed algorithm for mitigating PS, the initial phase involves detecting PS by calculating the fitness function. This function evaluates the error value to facilitate efficient power generation from the PV system. Consequently, the fitness function is formulated to equalize irradiance across the TCT PV array. The fitness function aims to optimize the configuration of PV panels to minimize row current and prevent bypass diode activation. The objective function of the proposed system is mathematically expressed as:

$$fitness = \text{minimize}\big(max\big(sum\ G(n,1)\big) - min\big(sum\ G(n,1)\big)\big) \quad (20)$$

If no PS is detected, reconfiguration is unnecessary. However, if PS is detected, the RTH algorithm initiates to determine the optimal positioning of PV modules. Initially, the algorithm generates a random arrangement of PV modules to commence the three phases: High Soaring, Low Soaring, and Stooping and Swooping. Upon meeting the termination criteria, the RTH algorithm provides the optimal PV array reconfiguration using switch control to initiate the MPPT. Figure 6 illustrates the comprehensive flowchart of the proposed strategy, encompassing the detection of PS followed by the reconfiguration of the PV array using the RTH algorithm.

### III.4 P&O MPPT CONTROL ALGORITHM

The Perturb and Observe (P&O) method is a straightforward iterative technique used for MPPT. This method perturbs the operating point of the PV system, causing the terminal voltage of the PV array to oscillate around the MPP voltage, even when solar irradiation and cell temperature remain constant. The flowchart of the P&O algorithm is depicted in Figure 7 [36].

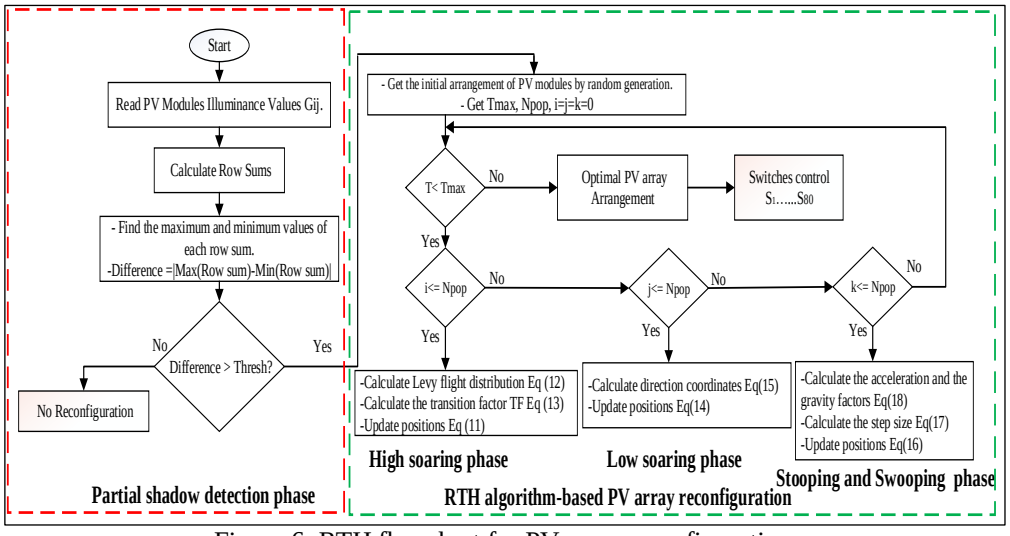


Figure 6: RTH flowchart for PV array reconfiguration.
Source: Authors, (2026).

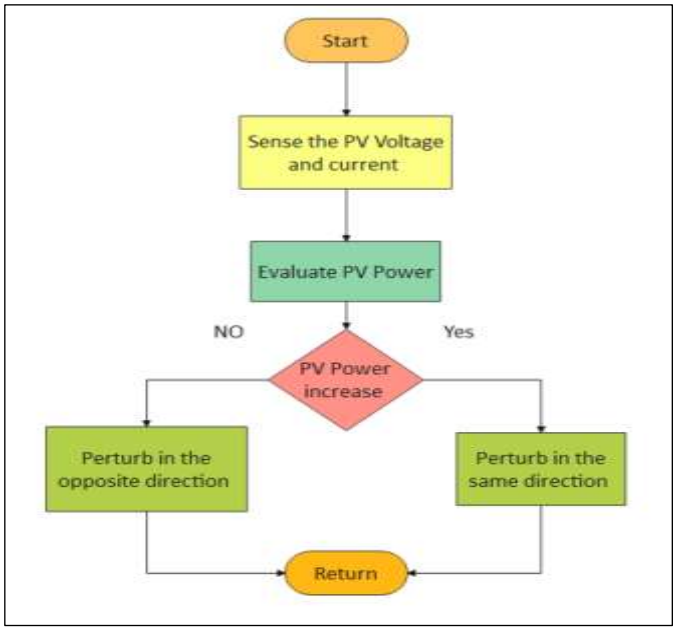


Figure 7: P&O algorithm Flowchart.
Source: Authors, (2026).

## IV. SIMULATION RESULTS

The performance of the proposed system is evaluated through MATLAB/Simulink simulations considering three partial shading conditions.

### IV.1 CASE 1

As shown in Figure 8(a), the 20-module PV array connected in a TCT configuration experiences uneven irradiance levels of 1000 W/m² and 600 W/m². In this scenario, substantial shading affects several modules, with the first row being the most impacted. The resulting arrangement is shown in Figure 8(b), which is employed to compute the output power. The switch matrix alters the module position to enhance the output power. The P-V characteristics of both configurations are represented in Figure 9. This figure demonstrates the effectiveness of the RTH-based reconfiguration approach in achieving a more uniform distribution of shadow levels across the PV array, resulting in consistent PV characteristics by minimizing the disparity in row currents. Particularly, by inspecting the P-V curve, it is seen that the power produced by the RTH (2.673 kW) outperforms that of the initial TCT interconnection (2.241 kW), with a single point of MPP instead of two MPP for the initial TCT arrangement, i.e., the lower number of MPP influenced the accuracy of the MPPT algorithm.

Figure 10 shows the response of the PV array power before and after reconfiguration based on the RTH algorithm. It is observed that PV array power increased by more than 19.27% after RTH reconfiguration. Note that the delay is due to the reconfiguration time of the PV array. Further, Figure 11 presents the electromagnetic torque, *Te*, response of the PV array with TCT reconfiguration and with RTH-based reconfiguration. The results highlight that the reconfiguration advantage in the electromagnetic torque results in a lower torque ripple. Moreover, Figure 12 shows the rotor speed evolution using the RTH reconfiguration technique. The findings demonstrate that the rotor speed after RTH PV array reconfiguration under PSC is better than (more than 1042 rpm) the initial configuration TCT without reconfiguration (998 rpm). The water flow evolution obtained is shown in Figure 13. It can be seen that the quantity of the pumped water under PSC using the proposed RTH algorithm reconfiguration is increased by more than 4,27 %.

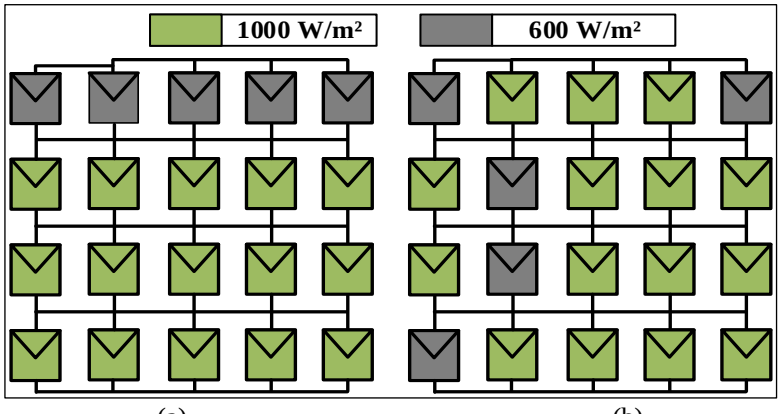


(a) (b)

Figure 8: Shading patterns for Case 1: (a) TCT configuration and (b) proposed RTH arrangement.
Source: Authors, (2026).

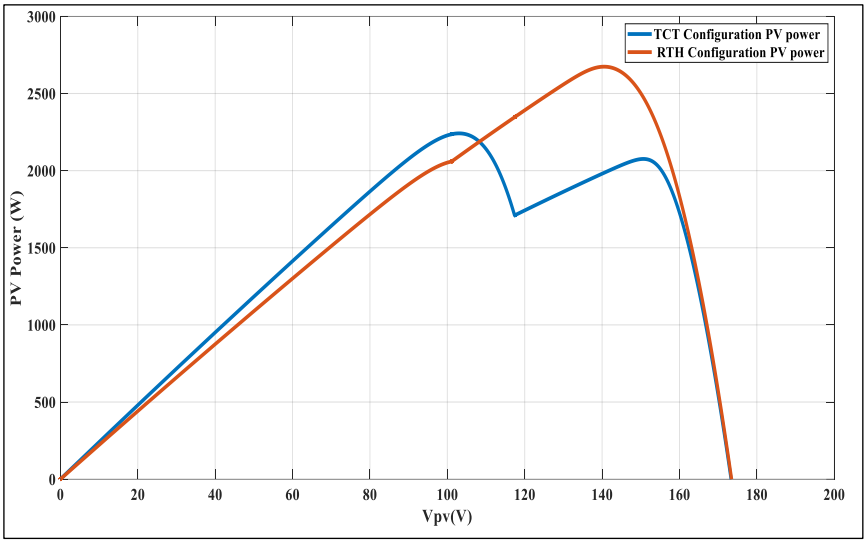


Figure 9: PV characteristics for Case 1 obtained using the TCT configuration and the proposed RTH algorithm.
Source: Authors, (2026).

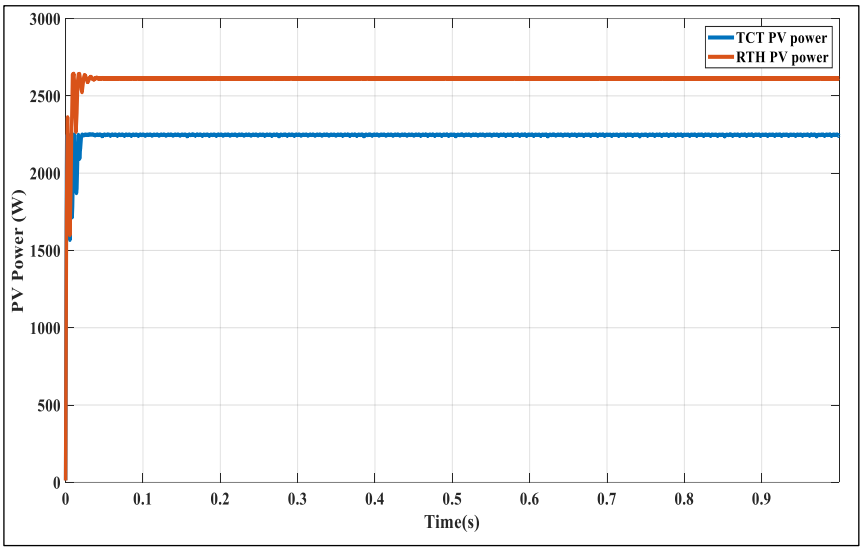


Figure 10: Comparison of PV array power for Case 1 under the conventional TCT interconnection and the proposed RTH-based reconfiguration.
Source: Authors, (2026).

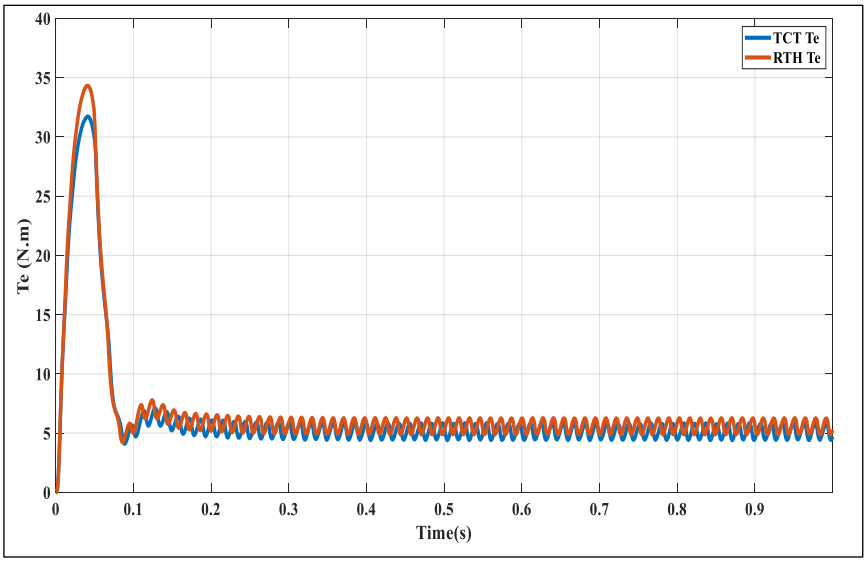


Figure 11: Motor electromagnetic torque for Case 1 before and after PV array reconfiguration.
Source: Authors, (2026).

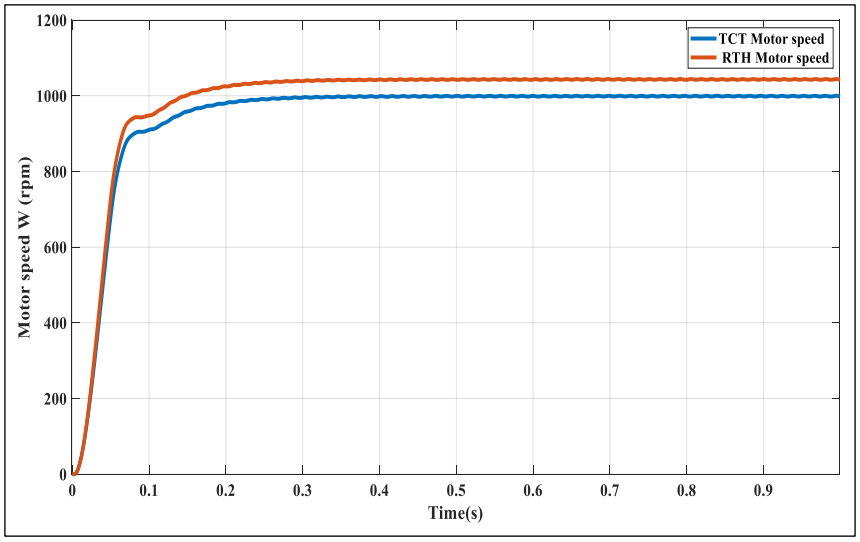


Figure 12: PV array power before (TCT interconnection) and after reconfiguration (RTH arrangement) for case 1.
Source: Authors, (2026).

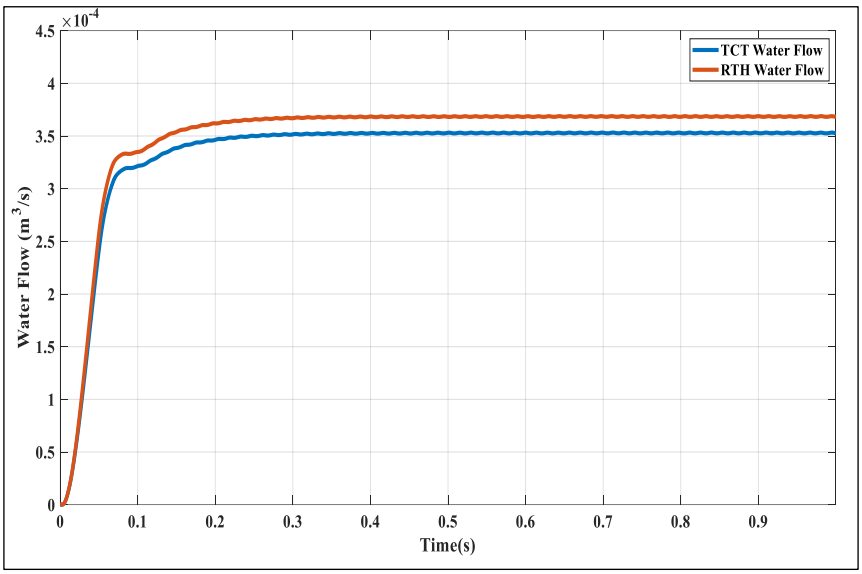


Figure 13: Comparison of PV array power for Case 1 under the conventional TCT interconnection and the proposed RTH-based reconfiguration.
Source: Authors, (2026).

## IV.2 CASE 2

Figure 14(a) shows the PV array interconnected in TCT under PSC. The PV array encounters three distinct irradiation levels: 300 W/m², 500 W/m², and 1000 W/m².The arrangement shown in Figure 14(b) provides a way to improve the power output using the proposed RTH algorithm. The repositioning of the PV modules is performed using the switch matrix. After reading the irradiance value of the PV modules, the proposed algorithm sends the switching states to the switching matrix, which changes the position of the module to improve the output power. In addition, Figure 15 displays the P-V characteristics in graphical form. This shows clearly the effectiveness of the RTH-based reconfiguration approach in achieving a more uniform distribution of shadow levels in the PV array, resulting in consistent PV characteristics by minimizing the disparity in row currents. Notably, upon inspecting the P-V curve, it becomes clear that the power produced by the RTH algorithm exceeds that of the original TCT interconnection, with only one point of maximum power MPP rather than two MPPs for the initial TCT arrangement; that is, the lesser number of MPPs affected the accuracy of the MPPT algorithm positively. Figure 16 illustrates the PV array power before and after applying the RTH-based reconfiguration.

The results show an increase in output power of over 42%, with a minor delay attributed to the reconfiguration time of the array. Additionally, the TCT configuration exhibits three local maximum power points (MPPs), where the conventional P&O MPPT algorithm fails to track the global MPP, producing approximately 1.470 kW instead of the optimal 2.100 kW. This highlights the critical influence of PV array topology on MPPT performance. Figure 17 compares the electromagnetic torque of the motor with and without PV array reconfiguration. The RTH-based approach effectively reduces torque ripple and enhances torque stability. Similarly, Figure 18 shows the rotor speed improvement achieved through the RTH reconfiguration, reaching over 980 rpm under partial shading conditions (PSCs), compared to a maximum of 889 rpm with the original TCT setup. Regarding water delivery, Figure 19 shows that implementing the RTH algorithm results in an increase of more than 11.57% in pumped water under PSCs. This notable improvement demonstrates the effectiveness of the proposed RTH-based reconfiguration strategy in enhancing the overall performance of PV water pumping systems.

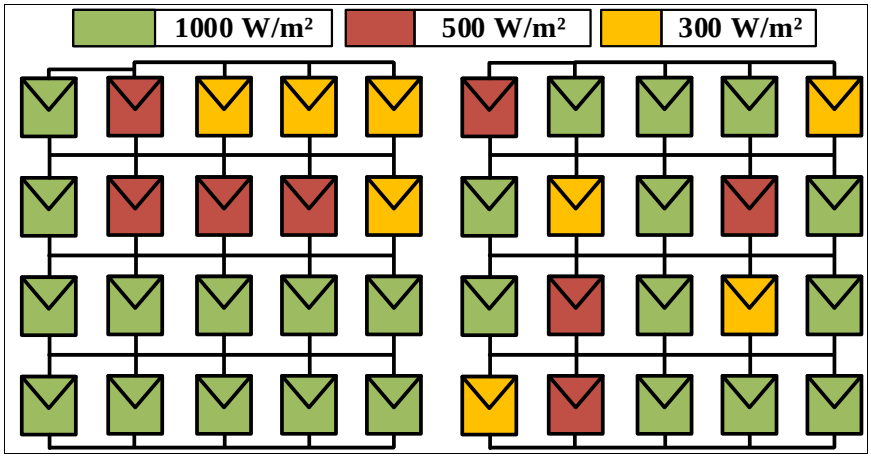


Figure 14: Illustration of shade dispersion in Case 2 under (a) the conventional TCT configuration and (b) the PV array with the proposed RTH reconfiguration.
Source: Authors, (2026).

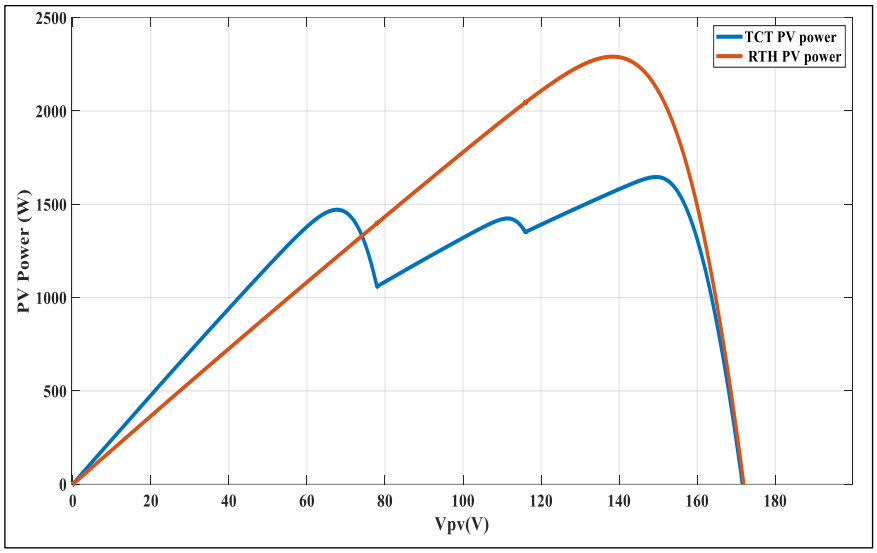


Figure 15: Comparison of PV characteristics for Case 2 under the conventional TCT configuration and the proposed BWO-based reconfiguration.
Source: Authors, (2026).

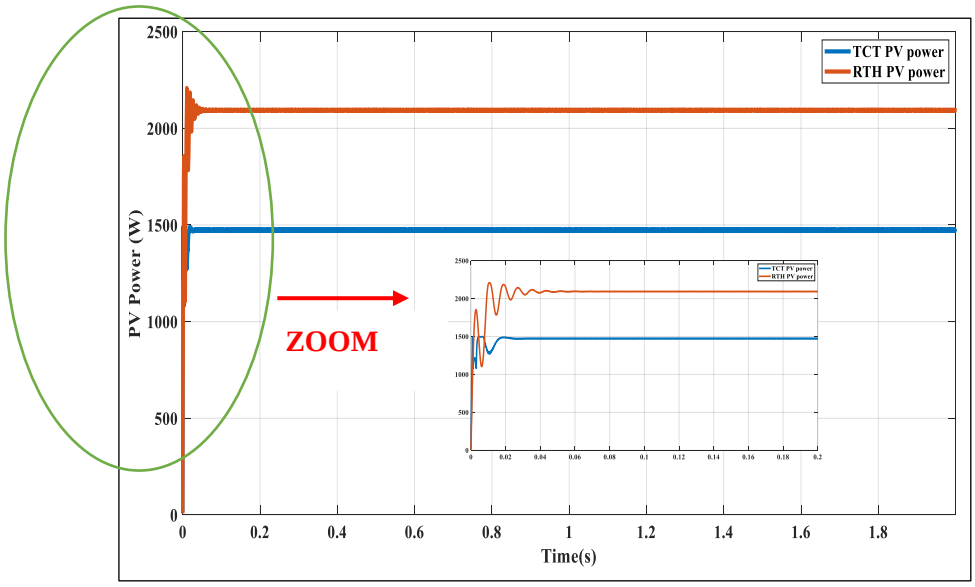


Figure 16: Comparison of PV array power for Case 2 under the conventional TCT interconnection and following RTH-based TCT reconfiguration.
Source: Authors, (2026).

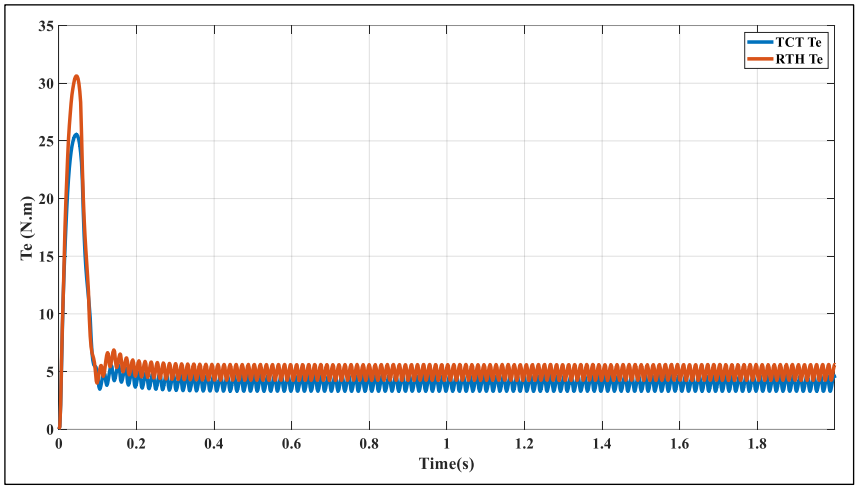


Figure 17: Comparison of motor electromagnetic torque for Case 2 under the original PV array configuration and after RTH-based reconfiguration.
Source: Authors, (2026).

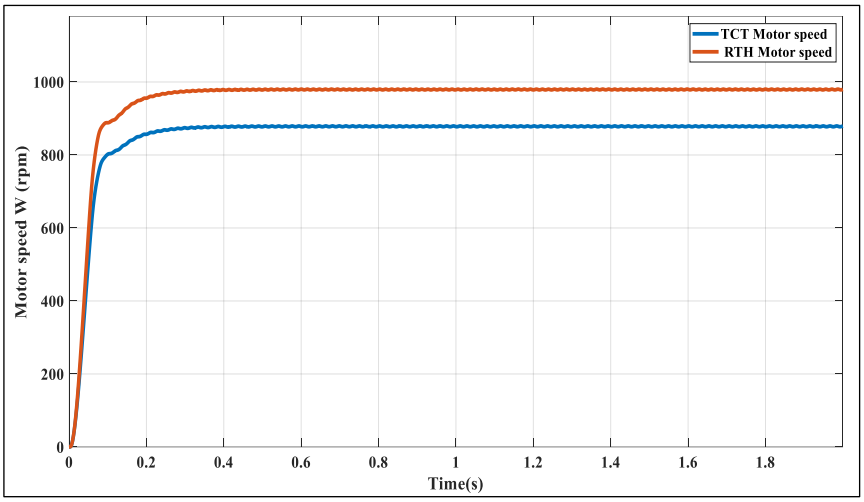


Figure 18: Comparison of motor speed for Case 2 under the original PV array configuration and following RTH-based reconfiguration.
Source: Authors, (2026).

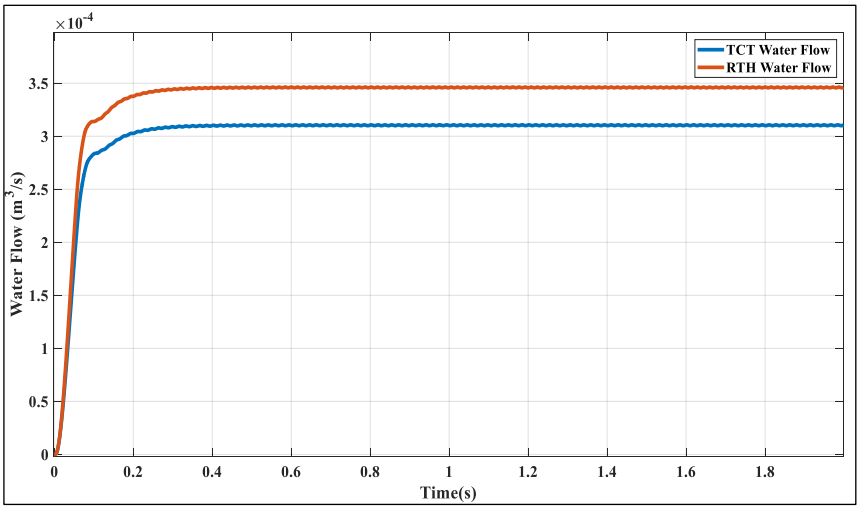


Figure 19: Comparison of water flow for Case 2 under the original PV array configuration and after RTH-based reconfiguration.
Source: Authors, (2026).

Table 3 presents a comparison of the overall performance indices of the PV water pumping system (PVWPS) under partial shading conditions (PSCs). The water gain for each scenario is computed using Equation (21), allowing an assessment of the effectiveness of the proposed reconfiguration strategy in enhancing water delivery under different shading patterns.

$$\text{Gained water (l/h)} = (Q_{RTH} - Q_{TCT}) \times 1000 \times 3600 \quad (21)$$

The performance indices in Table 3 clearly demonstrate the efficiency of the proposed algorithm. The system maintains stable steady-state operation and ensures satisfactory water delivery under partial shading (PS) conditions, while operating at the maximum power point (MPP). The results indicate a significant improvement in water flow, with average gains of 36 litres per hour in the first case and 111.6 liters per hour in the second case. This enhancement supports the development of sustainable photovoltaic water pumping systems in regions with limited access to conventional energy sources.

Table 3: Performance comparison of PVWPS under PSCs.

| N° | cases | Used technique | $P_{pv}$ (W) | W (rpm) | $T_e$ (N.m) | Q ($m^3/s)10^{-4}$ | Gained water (l/h) |
|---|---|---|---|---|---|---|---|
| 1 | Case 1 | Without reconfiguration (TCT) | 2243 | 999 | 5.01 | 3.5 | 36 |
| 2 | | With reconfiguration (RTH) | 2612 | 1042 | 5.21 | 3.6 | |
| 3 | Case 2 | Without reconfiguration (TCT) | 1476 | 877 | 3.33 | 3,09 | 111,6 |
| 4 | | With reconfiguration (RTH) | 2096 | 979 | 4.71 | 3,4 | |

Source: Authors, (2026).

## V. CONCLUSIONS

This research proposes a new control method for improving the water flow of a WPS based on PV under partial shadowing. In this proposed method, the RTHA optimization algorithm is adopted for dynamic PV array reconfiguration in an offline manner, considering PSCs. The MPPT-controlled reconfigured PV array is intended for supplying a BLDC motor-based WPS. The proposed control approach keeps PV systems near their MPP despite shading, thus improving power-voltage curves, efficiency, and water flow. The obtained results show a noticeable improvement in water delivery, with average gains of 36 liters per hour in the first operating case and 111.6 liters per hour in the second case. These improvements highlight the capability of the proposed approach to adapt the pumping operation to the available PV power while preserving system stability. Overall, this work contributes to the development of sustainable and efficient photovoltaic water pumping solutions, particularly suitable for remote and energy-constrained regions where access to conventional power sources is limited.

## VI. AUTHOR'S CONTRIBUTION

**Conceptualization:** Abdelouaoud Loukriz, Abderrahim Zemmit, Ahmed Bendib, Moadh Kichen.
**Methodology:** Abdelouaoud Loukriz, Abderrahim Zemmit, Ahmed Bendib, Moadh Kichen.
**Investigation:** Abdelouaoud Loukriz, Abderrahim Zemmit, Ahmed Bendib, Moadh Kichen.
**Discussion of results:** Abdelouaoud Loukriz, Abderrahim Zemmit, Ahmed Bendib, Moadh Kichen.
**Writing – Original Draft:** Abdelouaoud Loukriz, Ahmed Bendib.
**Writing – Review and Editing:** Abdelouaoud Loukriz, Ahmed Bendib.
**Resources:** Abdelouaoud Loukriz, Ahmed Bendib.
**Supervision:** Abdelouaoud Loukriz, Ahmed Bendib.
**Approval of the final text:** Abdelouaoud Loukriz, Ahmed Bendib.

## VII. REFERENCES

[1] A. Chaurey, P. M. Sadaphal, and D. Tyaqi, "Experiences with SPV water pumping systems for rural applications in India," Renew. Energy, vol. 3, no. 8, pp. 961–964, Nov. 1993, doi: 10.1016/0960-1481(93)90058-O.

[2] M. Mahmoud, "Experience results and techno-economic feasibility of using photovoltaic generators instead of diesel motors for water pumping from rural desert wells in Jordan," IEE Proc. C Gener. Transm. Distrib., vol. 137, no. 6, p. 391, 1990, doi: 10.1049/ip-c.1990.0053.

[3] S. S. Chandel, M. Nagaraju Naik, and R. Chandel, "Review of solar photovoltaic water pumping system technology for irrigation and community drinking water supplies," Renew. Sustain. Energy Rev., vol. 49, pp. 1084–1099, Sep. 2015, doi: 10.1016/j.rser.2015.04.083.

[4] H. Patel and V. Agarwal, "MATLAB-based modeling to study the effects of partial shading on PV array characteristics," IEEE Trans. Energy Convers., 2008, doi: 10.1109/TEC.2007.914308.

[5] A. Loukriz, M. Drif, A. Bouchelaghem, D. Saigaa, A. Bendib, and K. Moadh, "Current Balancing and PSO Methods-Based PV Array Output Power Optimization: A Comparative Study," in 2022 International Conference of Advanced Technology in Electronic and Electrical Engineering (ICATEEE), IEEE, Nov. 2022, pp. 1–6. doi: 10.1109/ICATEEE57445.2022.10093690.

[6] N. D. Kaushika and N. K. Gautam, "Energy yield simulations of interconnected solar PV arrays," in 2003 IEEE Power Engineering Society General Meeting (IEEE Cat. No.03CH37491), IEEE, 2004, pp. 2618–2618. doi: 10.1109/PES.2003.1271059.

[7] A. Loukriz, M. Kichene, A. Bendib, M. Drif, D. Saigaa, and H. Ahmed, "Improved dynamic reconfiguration strategy for power maximization of TCT interconnected PV arrays under partial shading conditions," Electr. Eng., pp. 1–12, Jun. 2024, doi: 10.1007/s00202-024-02529-y.

[8] D. La Manna, V. Li Vigni, E. Riva Sanseverino, V. Di Dio, and P. Romano, "Reconfigurable electrical interconnection strategies for photovoltaic arrays: A review," Renew. Sustain. Energy Rev., vol. 33, pp. 412–426, May 2014, doi: 10.1016/j.rser.2014.01.070.

[9] H. S. Sahu, S. K. Nayak, and S. Mishra, "Maximizing the Power Generation of a Partially Shaded PV Array," IEEE J. Emerg. Sel. Top. Power Electron., vol. 4, no. 2, pp. 626–637, Jun. 2016, doi: 10.1109/JESTPE.2015.2498282.

[10] G. Velasco-Quesada, F. Guinjoan-Gispert, R. Pique-Lopez, M. Roman-Lumbreras, and A. Conesa-Roca, "Electrical PV Array Reconfiguration Strategy for Energy Extraction Improvement in Grid-Connected PV Systems," IEEE Trans. Ind. Electron., vol. 56, no. 11, pp. 4319–4331, Nov. 2009, doi: 10.1109/TIE.2009.2024664.

[11] M. Matam, V. R. Barry, and A. R. Govind, “Optimized Reconfigurable PV array based Photovoltaic water-pumping system,” Sol. Energy, vol. 170, pp. 1063–1073, Aug. 2018, doi: 10.1016/j.solener.2018.05.046.

[12] J. P. Storey, P. R. Wilson, and D. Bagnall, “Improved optimization strategy for irradiance equalization in dynamic photovoltaic arrays,” IEEE Trans. Power Electron., vol. 28, no. 6, pp. 2946–2956, Jun. 2013, doi: 10.1109/TPEL.2012.2221481.

[13] M. Manjunath, B. Venugopal Reddy, and B. Lehman, “Performance improvement of dynamic PV array under partial shade conditions using M 2 algorithm,” IET Renew. Power Gener., vol. 13, no. 8, pp. 1239–1249, Jun. 2019, doi: 10.1049/iet-rpg.2018.5675.

[14] H. Rezk, A. Fathy, and M. Aly, “A robust photovoltaic array reconfiguration strategy based on coyote optimization algorithm for enhancing the extracted power under partial shadow condition,” Energy Reports, vol. 7, pp. 109–124, Nov. 2021, doi: 10.1016/j.egyr.2020.11.035.

[15] B. Aljafari, P. R. Satpathy, and S. B. Thanikanti, “Partial shading mitigation in PV arrays through dragonfly algorithm based dynamic reconfiguration,” Energy, vol. 257, p. 124795, Oct. 2022, doi: 10.1016/j.energy.2022.124795.

[16] A. Fathy, “Recent meta-heuristic grasshopper optimization algorithm for optimal reconfiguration of partially shaded PV array,” Sol. Energy, vol. 171, pp. 638–651, Sep. 2018, doi: 10.1016/j.solener.2018.07.014.

[17] R. Cao et al., “Photovoltaic array reconfiguration under partial shading conditions based on ant colony optimization,” in 2020 Chinese Control And Decision Conference (CCDC), IEEE, Aug. 2020, pp. 703–708. doi: 10.1109/CCDC49329.2020.9164084.

[18] M. Palpandian, D. P. Winston, B. P. Kumar, C. S. Kumar, T. S. Babu, and H. H. Alhelou, “A New Ken-Ken Puzzle Pattern Based Reconfiguration Technique for Maximum Power Extraction in Partial Shaded Solar PV Array,” IEEE Access, 2021, doi: 10.1109/ACCESS.2021.3076608.

[19] G. Meerimatha and B. L. Rao, “Genetic Algorithm Based PV Array Reconfiguration for Improving Power Output under Partial Shadings,” Int. J. Renew. Energy Res., no. v10i2, 2020, doi: 10.20508/ijrer.v10i2.10731.g7971.

[20] R. Kumar Pachauri et al., “Study on Meta-heuristics techniques for shade dispersion to enhance GMPP of PV array systems under PSCs,” Sustain. Energy Technol. Assessments, 2023, doi: 10.1016/j.seta.2023.103353.

[21] T. S. Babu, J. P. Ram, T. Dragicevic, M. Miyatake, F. Blaabjerg, and N. Rajasekar, “Particle Swarm Optimization Based Solar PV Array Reconfiguration of the Maximum Power Extraction Under Partial Shading Conditions,” IEEE Trans. Sustain. Energy, vol. 9, no. 1, pp. 74–85, Jan. 2018, doi: 10.1109/TSTE.2017.2714905.

[22] D. Yousri, D. Allam, and M. B. Eteiba, “Optimal photovoltaic array reconfiguration for alleviating the partial shading influence based on a modified harris hawks optimizer,” Energy Convers. Manag., vol. 206, p. 112470, Feb. 2020, doi: 10.1016/j.enconman.2020.112470.

[23] A. Fathy, D. Yousri, T. S. Babu, H. Rezk, and H. S. Ramadan, “An enhanced reconfiguration approach for mitigating the shading effect on photovoltaic array using honey badger algorithm,” Sustain. Energy Technol. Assessments, 2023, doi: 10.1016/j.seta.2023.103179.

[24] D. C. Huynh, L. D. Ho, M. W. Dunnigan, and C. Barbalata, “Solar Photovoltaic Array Reconfiguration for Optimizing Harvested Power Using an Advanced Artificial Bee Colony Algorithm,” in Proceedings of 2023 International Conference on System Science and Engineering, ICSSE 2023, 2023. doi: 10.1109/ICSSE58758.2023.10227209.

[25] C. Baby T, V. S. Sabah, K. P. Lall, and A. Chitra, “Multilevel inverter fed induction motor drive for pumping application,” in 2015 International Conference on Technological Advancements in Power and Energy (TAP Energy), IEEE, Jun. 2015, pp. 85–92. doi: 10.1109/TAPENERGY.2015.7229597.

[26] M. Errouha, A. Derouich, B. Nahid-Mobarakeh, S. Motahhir, and A. El Ghzizal, “Improvement control of photovoltaic based water pumping system without energy storage,” Sol. Energy, vol. 190, pp. 319–328, Sep. 2019, doi: 10.1016/j.solener.2019.08.024.

[27] X. Lufei and N. Guangqun, “Research on Direct Torque Control of Induction Motor Based on TMS320LF2407A,” Phys. Procedia, vol. 25, pp. 513–519, Jan. 2012, doi: 10.1016/j.phpro.2012.03.119.

[28] R. Kumar and B. Singh, “Single Stage Solar PV Fed Brushless DC Motor Driven Water Pump,” IEEE J. Emerg. Sel. Top. Power Electron., vol. 5, no. 3, pp. 1377–1385, Sep. 2017, doi: 10.1109/JESTPE.2017.2699918.

[29] R. Kumar and B. Singh, “BLDC Motor-Driven Solar PV Array-Fed Water Pumping System Employing Zeta Converter,” IEEE Trans. Ind. Appl., vol. 52, no. 3, pp. 2315–2322, May 2016, doi: 10.1109/TIA.2016.2522943.

[30] S. Sashidhar, V. Guru Prasad Reddy, and B. G. Fernandes, “A Single-Stage Sensorless Control of a PV-Based Bore-Well Submersible BLDC Motor,” IEEE J. Emerg. Sel. Top. Power Electron., 2019, doi: 10.1109/JESTPE.2018.2810506.

[31] A. LOUKRIZ, “Contribution au Développement de Techniques de Recherche de la Topologie Optimale d’un Générateur Photovoltaïque,” Biskra University, 2022. Accessed: Aug. 14, 2023. [Online]. Available: http://thesis.univ-biskra.dz/5806.

[32] M. M. Shebani and T. Iqbal, “Dynamic Modeling, Control, and Analysis of a Solar Water Pumping System for Libya,” J. Renew. Energy, vol. 2017, pp. 1–13, 2017, doi: 10.1155/2017/8504283.

[33] A. Saoudi, S. Krim, and M. F. Mimouni, “Enhanced Intelligent Closed Loop Direct Torque and Flux Control of Induction Motor for Standalone Photovoltaic Water Pumping System,” Energies, vol. 14, no. 24, p. 8245, Dec. 2021, doi: 10.3390/en14248245.

[34] S. Djeriou, A. Kheldoun, and A. Mellit, “Efficiency Improvement in Induction Motor-Driven Solar Water Pumping System Using Golden Section Search Algorithm,” Arab. J. Sci. Eng., vol. 43, no. 6, pp. 3199–3211, Jun. 2018, doi: 10.1007/s13369-017-2972-6.

[35] A. M. Ajmal, T. Sudhakar Babu, V. K. Ramachandaramurthy, D. Yousri, and J. B. Ekanayake, “Static and dynamic reconfiguration approaches for mitigation of partial shading influence in photovoltaic arrays,” Sustain. Energy Technol. Assessments, vol. 40, p. 100738, Aug. 2020, doi: 10.1016/j.seta.2020.100738.

[36] N. Femia, G. Petrone, G. Spagnuolo, and M. Vitelli, “Optimization of Perturb and Observe Maximum Power Point Tracking Method,” IEEE Trans. Power Electron., vol. 20, no. 4, pp. 963–973, Jul. 2005, doi: 10.1109/TPEL.2005.850975.